

## REVIEW ARTICLE

# Numerical optimization of the mixing flow in a straight tube, single, and two loops helical coil

Wameath S. Abdul-Majeed\*

Department of Chemical and Petrochemical Engineering – University of Nizwa,  
PC616, Nizwa – Oman

## ABSTRACT

A great interest of using curved pipes was shown in the industrial applications due to many advantages such as developed agitation which can be obtained as an alternative to the conventional agitation at lower energy consumption and reduced cost. A computational investigations were conducted in this study to contemplate on the enhancement occur in the mixing flow upon using single and multi loops helical coil compared with a straight tube. The objective was to optimize the number of loops in the helical coil. The computations were achieved via “Fluent software” in which 3d, second order upwind were used for all cases studied. The study consisted of four parts in which the numerical error study was conducted in the first part to optimize the grid meshing and to make sure that the results are independent of it. The effect of using the helical coil on the pressure drop was conducted in the second part. The third and fourth parts of the study were devoted to envisage the enhancement of applying the curved loops in the coil on the heat and mass transfer, respectively. The main findings of the study were limited effect of single loop coil on the heat and mass transfer processes. Better effect was depicted upon increasing the number of loops in the helical coil into 2. However, applying 2 loops has resulted in building up higher pressure drops. Moreover, the pressure drop was shown slightly higher in the case of applying water when compared with air.

**Keywords:** mixing flow; flow in curved sections; swirl flow; helical coil; passive flow techniques

## Introduction

Flow in curved section has been identified as a passive technique that could enhance transport phenomena<sup>[1]</sup>. In 1927, Dean<sup>[2]</sup> has reported for the first time the characteristics of flow in a curved section. He denoted that a flow pattern in a helical coil is complicated due to the formation of secondary flow. He stated that a pair of symmetric vortices is formed on the cross sectional plane due to centrifugal force.

The strength of secondary flow is characterized by Dean number.

$$De = Re \sqrt{a/R_c}$$

where  $Re$ ,  $R_c$  and  $a$  are Reynolds number, coil radius and tube radius, respectively.

This kind of flow pattern is known to impart better contact between the surface of the tube and fluids due to the formation of swirl which leads to mixing the fluid and improves the mass and momentum diffusion coefficients as well as the temperature gradient. For heating and mass transfer applications, the advantages were demonstrated by increasing the transfer rate and providing higher heat and mass transfer area per unit volume of space. Using curved tubes in specific reaction applications was marked with homogenization of feed streams with a minimum residence time<sup>[3]</sup>. It was mentioned in the literature that using the helical coil instead of the straight tube for continuous flow problems enhanced the degree of mixing and reduced the required tube length by 20% for Newtonian fluid in laminar flow<sup>[4]</sup>.

Hence, voluminous number of papers, published through nine decades, have discussed the transport phenomena in curved section from different perspectives. Many of these papers highlighted enhancement on the heat exchanger performance upon enforcing flow in a traditional helical section<sup>[5-7]</sup>. Other papers discussed the fluid flow and heat transfer in concentric helical section and other configurations<sup>[8-12]</sup>. The geometry of the helical section was found quite

critical on enhancements in momentum, mass and heat transfer. Several configuration parameters such as length of spiral pipes, number of turns, coil radius, helix diameter were studied by several research groups<sup>[13–15]</sup>. In studies of helical double heat exchanger, it was found that heat transfer increased by increasing the inner Dean number, inner tube diameter, curvature ratio, and by the reduction of the pitch of the heat exchanger coil<sup>[14]</sup>. In regards to the number of loops in the helical coil, Jassim<sup>[16]</sup> has tested two coils of same length and different number of loops, 5 and 10. He reported that increasing the number of loops per unit length of spiral coil enhances the rate of heat transfer through spiral coil heat exchanger. In contrast, Ranjbar and Seyyedvalilu<sup>[14]</sup> reported that increasing the number of loops in a double tube exchanger led to a significant decreases in the heat transfer coefficient. They denoted that increasing the number of coils from 1 to 6 led to a 80% decrease in the estimated overall heat transfer coefficient. On the other side, CFD study and experimental investigations, conducted in our previous work<sup>[17]</sup>, have discussed the application of helical section for separation of gaseous species from carrying liquid. The results have shown that two loops helical section was sufficient to achieve the full separation of arsenic hydride and the hydrogen gas from the liquid phase and their transfer into the accompanying gas phase.

To the author knowledge, no clue is shown in the literature that could present a guideline to contemplate on the number of loops and its reflections on the helical tube performance. Hence, this study is dedicated for this purpose and to elucidate the effect of increasing the number of loops on the transport properties. It's worth noting that a considerable time was consumed to complete this study, as the computations were conducted through a personal computer and most of the cases studied took several hours to converge. This limitation was the reason for adopting no more than 2 loops helical coil. The study consisted of four parts. In the first part, a systematic error estimation for the pressure drop computation was conducted in order to verify the certainty of the solutions obtained. The second part was dedicated to study the effect of using the helical coil on the pressure drop as well as computing the radial and axial pressure drop in the curved section of the coil. The computation were achieved using air and water separately in order to conceive the effect of the fluid type on the process. The third part was dedicated to envisage the effect of using single loop coil on the heat transfer process. The computations in this part were achieved using water which was assumed to be introduced into the mixing section from two inlets with different temperatures. The fourth part was devoted to study the effect of using the coil on the mass transfer process. A mixture of (Ethanol-water) was assumed to be introduced into the mixing section from the bottom inlet while the top inlet was used to introduce a stream of pure water. The computations were achieved by using “Fluent software” in which 3d, second order upwind, proper grid meshing and sufficient number of iterations were used for all the cases studied.

## Problem Statement

It is assumed that two streams (A&B) are introduced into the mixing section through (T-junction), where each of these streams enters at one of the T-junction sides. The mixing section is studied in three cases; the first is a straight tube while the second is helical coil composed of one loop and the third is helical coil of 2 loops. The schematic diagram for straight tube and one loop coil is shown in Figure 1.

## Mathematical Model

It is assumed that the flow is applied in terms of Cartesian coordinates with steady state conditions and constant transport properties.

Symbols :

$u$  : the velocity in the (x) direction

$v$  : the velocity in the (y) direction

$w$  : the velocity in the (z) direction

$\rho$  : density

$\mu$  : viscosity

The mathematical description for the flow problem is shown as follows:

- Continuity equation :

In case of steady flow and constant density, the continuity equation becomes:

$$\frac{\partial \rho}{\partial t} + \frac{\partial \rho u_j}{\partial x_j} = 0$$

$$\frac{\rho \partial u_j}{\partial x_j} = 0, \text{ since } \rho \text{ non zero} \rightarrow \frac{\partial u_j}{\partial x_j} = 0 \quad \dots (a)$$

Expanding equation (a) gives the following:

$$\frac{\partial u_j}{\partial x_j} = \frac{\partial u}{\partial x} + \frac{\partial v}{\partial y} + \frac{\partial w}{\partial z} = 0 \quad \dots (a1)$$

- Momentum equation: (steady state, no gravity effect , constant density and viscosity)

$$\frac{\partial \rho u_i}{\partial t} + \frac{\partial \rho u_j u_i}{\partial x_j} = \frac{-\partial p}{\partial x_i} + \frac{\partial}{\partial x_j} \left[ u \left( \frac{\partial u_i}{\partial x_j} + \frac{\partial u_j}{\partial x_i} \right) \right] \quad \dots(b)$$

$$\frac{\partial \rho u_i}{\partial t} + \frac{\partial \rho u_j u_i}{\partial x_j} = \frac{-\partial p}{\partial x_i} u \left[ \frac{\partial^2 u_i}{\partial x_j^2} + \frac{\partial}{\partial x_i} \left( \frac{\partial u_j}{\partial x_j} \right) \right]$$

Since  $\frac{\partial u_j}{\partial x_j} = 0$  (constant density) &  $\frac{\partial \rho u_i}{\partial t} = 0$  (steady state)

Equation (b) becomes:

$$\frac{\rho \partial u_j u_i}{\partial x_j} = \frac{-\partial p}{\partial x_i} + \frac{\mu \partial^2 u_i}{\partial x_j^2} \quad \dots (b1)$$

Expanding equation (b1) gives the following:

- x – momentum :

$$\frac{\rho \partial uu}{\partial x} + \frac{\rho \partial vu}{\partial y} + \frac{\rho \partial wu}{\partial z} = \frac{-\partial p}{\partial x} + \mu \left[ \frac{\partial^2 u}{\partial x^2} + \frac{\partial^2 u}{\partial y^2} + \frac{\partial^2 u}{\partial z^2} \right] \quad \dots (b2)$$

- y – momentum :

$$\frac{\rho \partial uv}{\partial x} + \frac{\rho \partial vv}{\partial y} + \frac{\rho \partial wv}{\partial z} = \frac{-\partial p}{\partial y} + \mu \left[ \frac{\partial^2 v}{\partial x^2} + \frac{\partial^2 v}{\partial y^2} + \frac{\partial^2 v}{\partial z^2} \right] \quad \dots(b3)$$

- z – momentum :

$$\frac{\rho \partial uw}{\partial x} + \frac{\rho \partial vw}{\partial y} + \frac{\rho \partial ww}{\partial z} = \frac{-\partial p}{\partial z} + \mu \left[ \frac{\partial^2 w}{\partial x^2} + \frac{\partial^2 w}{\partial y^2} + \frac{\partial^2 w}{\partial z^2} \right] \quad \dots(b4)$$

In order to introduce the dimensionless quantities, we choose characteristics fixed scales for length  $L_0$  and velocity  $V_0$ . The variables in above equations can be identified by using these fixed scales as follows:

$$\underline{u}^* = \frac{u}{V_0}, \underline{v}^* = \frac{v}{V_0}, \underline{w}^* = \frac{w}{V_0}, \underline{x}^* = \frac{x}{L_0}, \underline{y}^* = \frac{y}{L_0}, \underline{z}^* = \frac{z}{L_0}$$

$$\underline{p}^* = \frac{p}{\rho V_0^2} \quad (\text{where } \rho = \text{constant density})$$

Multiplying both sides of equation (a1) by  $(L_0 / V_0)$  produces the following equation:

$$\frac{\partial \underline{u}^*}{\partial \underline{x}^*} + \frac{\partial \underline{v}^*}{\partial \underline{y}^*} + \frac{\partial \underline{w}^*}{\partial \underline{z}^*} = 0 \quad \dots (aa1)$$

Multiplying both sides of equations (b2) , (b3) and (b4) by  $(L_0 / (V_0)^2)$  produce the following dimensionless equations:

$$\frac{\partial \underline{u}^* \underline{u}^*}{\partial \underline{x}^*} + \frac{\partial \underline{v}^* \underline{u}^*}{\partial \underline{y}^*} + \frac{\partial \underline{w}^* \underline{u}^*}{\partial \underline{z}^*} = \frac{-\partial \underline{p}^*}{\partial \underline{x}^*} + \frac{\mu}{\rho L_0 V_0} \left[ \frac{\partial}{\partial \underline{x}^*} \left( \frac{\partial \underline{u}^*}{\partial \underline{x}^*} \right) + \frac{\partial}{\partial \underline{y}^*} \left( \frac{\partial \underline{u}^*}{\partial \underline{y}^*} \right) + \frac{\partial}{\partial \underline{z}^*} \left( \frac{\partial \underline{u}^*}{\partial \underline{z}^*} \right) \right], \text{or}$$

$$\frac{\partial \underline{u}^* \underline{u}^*}{\partial \underline{x}^*} + \frac{\partial \underline{v}^* \underline{u}^*}{\partial \underline{y}^*} + \frac{\partial \underline{w}^* \underline{u}^*}{\partial \underline{z}^*} = \frac{-\partial \underline{p}^*}{\partial \underline{x}^*} + \frac{1}{\text{Re}} \left[ \frac{\partial}{\partial \underline{x}^*} \left( \frac{\partial \underline{u}^*}{\partial \underline{x}^*} \right) + \frac{\partial}{\partial \underline{y}^*} \left( \frac{\partial \underline{u}^*}{\partial \underline{y}^*} \right) + \frac{\partial}{\partial \underline{z}^*} \left( \frac{\partial \underline{u}^*}{\partial \underline{z}^*} \right) \right] \quad \dots(bb2)$$

$$\frac{\partial \underline{u}^* \underline{v}^*}{\partial \underline{x}^*} + \frac{\partial \underline{v}^* \underline{v}^*}{\partial \underline{y}^*} + \frac{\partial \underline{w}^* \underline{v}^*}{\partial \underline{z}^*} = \frac{-\partial \underline{p}^*}{\partial \underline{y}^*} + \frac{1}{\text{Re}} \left[ \frac{\partial}{\partial \underline{x}^*} \left( \frac{\partial \underline{v}^*}{\partial \underline{x}^*} \right) + \frac{\partial}{\partial \underline{y}^*} \left( \frac{\partial \underline{v}^*}{\partial \underline{y}^*} \right) + \frac{\partial}{\partial \underline{z}^*} \left( \frac{\partial \underline{v}^*}{\partial \underline{z}^*} \right) \right] \quad \dots(bb3)$$

$$\frac{\partial \underline{u}^* \underline{w}^*}{\partial \underline{x}^*} + \frac{\partial \underline{v}^* \underline{w}^*}{\partial \underline{y}^*} + \frac{\partial \underline{w}^* \underline{w}^*}{\partial \underline{z}^*} = \frac{-\partial \underline{p}^*}{\partial \underline{z}^*} + \frac{1}{\text{Re}} \left[ \frac{\partial}{\partial \underline{x}^*} \left( \frac{\partial \underline{w}^*}{\partial \underline{x}^*} \right) + \frac{\partial}{\partial \underline{y}^*} \left( \frac{\partial \underline{w}^*}{\partial \underline{y}^*} \right) + \frac{\partial}{\partial \underline{z}^*} \left( \frac{\partial \underline{w}^*}{\partial \underline{z}^*} \right) \right] \quad \dots(bb4)$$

- Boundary conditions :

In the case of inlet boundary conditions, the values of velocity are known for the two inlets of the (T-junction), while the pressure at outlet edge is zero.

The inlet velocities at both T-junction sides can be normalized to get the following:

$$V_1^* = V_1/V_0, \quad V_2^* = V_2/V_0,$$

The above equations were applicable in the first part of the study, where the effect of using the coil on the pressure drop is studied without imposing effect of the heat and mass transfer.

In order to study the effect of using the coil on the heat and mass transfer rates, a mathematical description was given by using the energy and species equations as follows:

- Energy equation : ( small mach number, uniform Cp & λ , non uniform ρ )

$$\frac{\partial \rho C_p T}{\partial t} + \frac{\partial \rho u_j C_p T}{\partial x_j} = \frac{\lambda \partial}{\partial x_j} \left[ \frac{\partial T}{\partial x_j} \right] \quad \dots\dots (c)$$

In the case of steady state conditions, the first term of equation (c) is neglected then expanding the equation to give:

$$\frac{\partial \rho u C_p T}{\partial x} + \frac{\partial \rho v C_p T}{\partial y} + \frac{\partial \rho w C_p T}{\partial z} = \lambda \left[ \frac{\partial^2 T}{\partial x^2} + \frac{\partial^2 T}{\partial y^2} + \frac{\partial^2 T}{\partial z^2} \right]$$

- Species k equation : ( uniform Dk & non uniform ρ )

$$\frac{\partial \rho Y_K}{\partial t} + \frac{\partial \rho u_j Y_K}{\partial x_j} = \frac{D_K \partial}{\partial x_j} \left[ \frac{\rho \partial Y_K}{\partial x_j} \right] \quad \dots\dots (d)$$

In the case of steady state, the first term of equation (d) is neglected, then expanding the equation to give:

$$\frac{\partial \rho u Y_K}{\partial x} + \frac{\partial \rho v Y_K}{\partial y} + \frac{\partial \rho w Y_K}{\partial z} = D_K \left[ \frac{\partial}{\partial x} \left( \frac{\rho \partial Y_K}{\partial x} \right) + \frac{\partial}{\partial y} \left( \frac{\rho \partial Y_K}{\partial y} \right) + \frac{\partial}{\partial z} \left( \frac{\rho \partial Y_K}{\partial z} \right) \right] \quad \dots (d1)$$

The dimensionless forms of the energy and species equations are obtained after defining the following dimensionless quantities:

$$u^* = u/V_0, \quad v^* = v/V_0, \quad w^* = w/V_0, \quad p^* = p/p_0$$

$$x^* = x/L_0, \quad y^* = y/L_0, \quad z^* = z/L_0, \quad T^* = T/T_0, \quad h^* = h/C_p T_0,$$

where:  $h = C_p T$

Multiplying both sides of energy equation (c1) by  $(L_0 / (\rho_0 V_0 C_p T_0))$  gives :

$$\frac{\partial p^* u^* h^*}{\partial x^*} + \frac{\partial p^* v^* h^*}{\partial y^*} + \frac{\partial p^* w^* h^*}{\partial z^*} = \frac{\lambda}{\rho_0 V_0 C_p L_0} \left[ \frac{\partial (\partial T^*)}{\partial x^* \partial x^*} + \frac{\partial (\partial T^*)}{\partial y^* \partial y^*} + \frac{\partial (\partial T^*)}{\partial z^* \partial z^*} \right] \quad \dots (c2)$$

where:  $\lambda / \rho_0 V_0 C_p L_0 = 1/Re Pr = 1/PeE$

Multiplying both sides of species equation (d1) by  $(L_0 / (\rho_0 V_0 Y_0))$  gives :

$$\frac{\partial p^* u^* Y_K^*}{\partial x^*} + \frac{\partial p^* v^* Y_K^*}{\partial y^*} + \frac{\partial p^* w^* Y_K^*}{\partial z^*} = \frac{D_K}{L_0 V_0} \left[ \frac{\partial}{\partial x^*} \left( \frac{\partial p^* T^*}{\partial x^*} + \frac{\partial p^* T^*}{\partial y^*} + \frac{\partial p^* T^*}{\partial z^*} \right) \right]$$

Where :  $D_K / V_0 L_0 = 1/Re Sc = 1/PeM$

- Boundary conditions : ( Insulated wall + known inlet conditions )

The values of temperature and species concentration are known for the two inlets of the (T-junction), thus:

The inlet temperature and species concentration at both T-junction sides can be normalized to get the following dimensionless values:

$$T_1^* = T_1/T_0, \quad T_2^* = T_2/T_0,$$

$$Y_{K1}^* = Y_{K1}/Y_0, \quad Y_{K2}^* = Y_{K2}/Y_0$$

## Solution Steps

The system configuration has been sketched using Gambit software as shown in **Figure 1**. For the case of 2 loops coil (not shown in **Figure 1**), two turns of a helical coil (1.0 mm ID) with a top and bottom turn radius of  $(R=1 \text{ mm})$  and 19.06 mm total assembly length, is applied. The case files exported to Fluent with specific grid size (Tet/ Hybrid mesh type) for each case. (3d), second order upwind, and  $(1 \cdot 10^{-10})$  residuals were set in Fluent in order to get the required accuracy for solution.

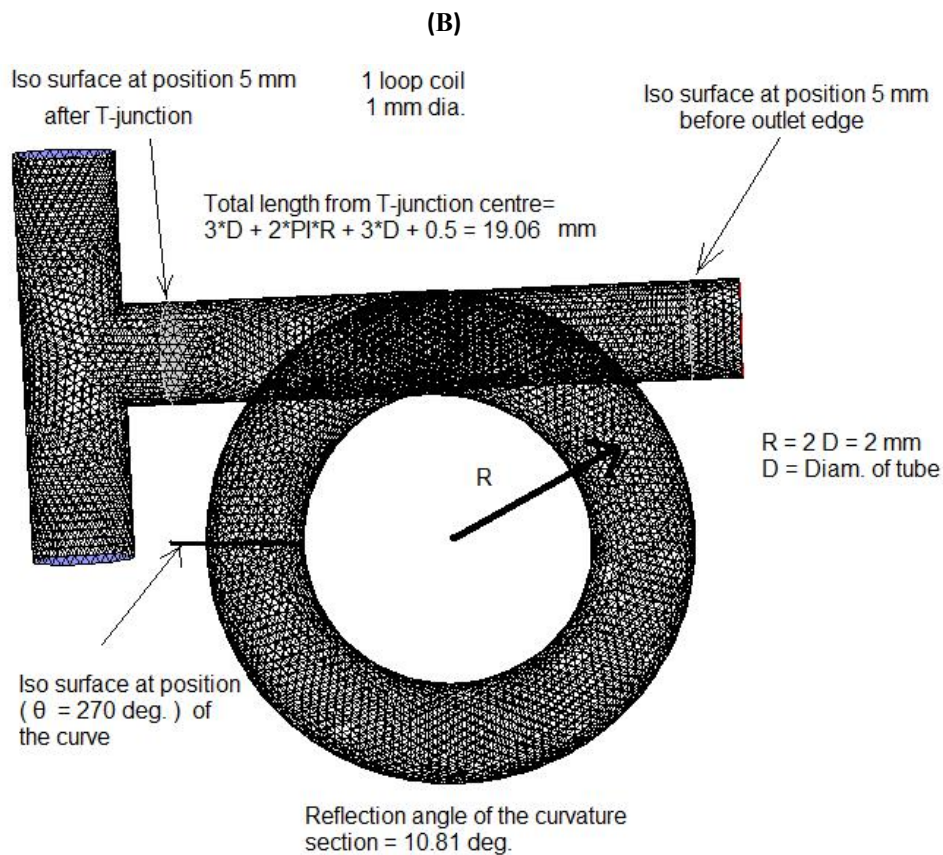
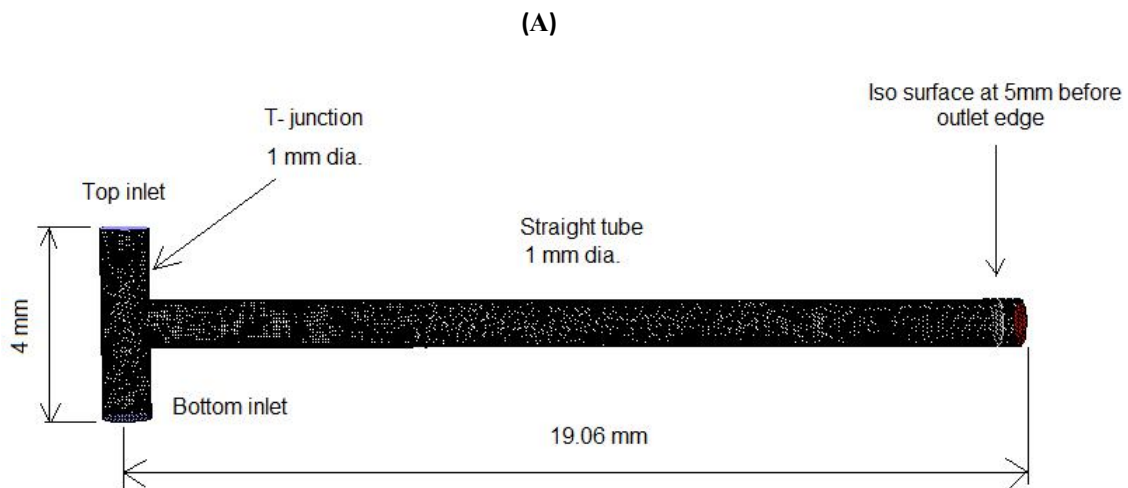


**Figure 1.** Schematic diagram of the used systems/(A) Straight tube (B) 1 loop coil

## Numerical Error Study

In the first part of the study, a systematic error estimation study for the pressure drop computation was conducted to conclude the solutions certainty. Ambient air with the same velocity was assumed to be introduced into both T-junction sides. Similar positions were selected for computing the pressure drop for both straight tube and 1 loop coil. The first position was 0.5 mm after the T-junction, the other one was 0.5 mm before the outlet edge.

Table 1 and Table 2 illustrate the computed pressure drop and the relative error that obtained for each grid cell size. The solution (pressure drop) was calculated at position 0.5 mm before the tube outlet edge. The relative error was calculated as: Relative error = [solution of last iteration – solution of specific iteration (where low changes were observed)]/solution of last iteration.

**Table 1.** Error study for a straight tube

Grid cell size (mm)	No. Of iterations	Pressure drop (Pascal)	Relative error
0.35	1500	1.6630599570	0
0.25	1500	1.748827170	1.7154E-09
0.2	1500	1.769689221	3.955E-09
0.15	1500	1.793573275	1.092E-07
0.1	1500	1.82076706	3.174E-07
0.08	1500	1.822852907	2.088E-06
0.06	1500	1.823354168	2.1109E-05

**Table 2.** Error study for single loop coil

Grid cell size (mm)	No. Of iterations	Pressure drop (Pascal)	Relative error *
0.30	1000	1.67118635	1.908E-07
0.15	1000	1.792641809	4.462E-09
0.10	1000	1.814044266	6.670E-07
0.08	1000	1.821950417	7.818E-06
0.06	1000	1.82817622	2.082E-05
0.04	1000	1.833953415	6.898E-04
0.0325	1040	1.836824	3.403E-04

Figure 2 and Figure 3 represent the convergence history of the solution for three grid cells.

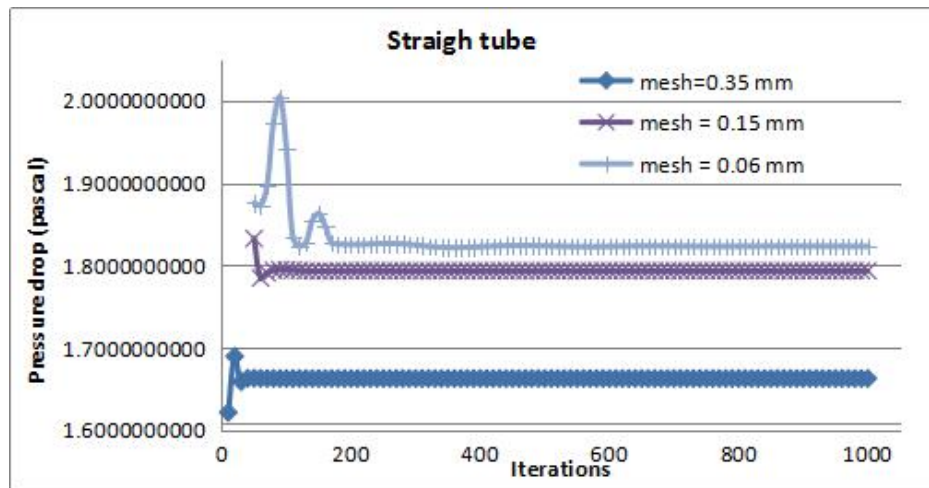


**Figure 2.** Solution convergence history/Straight tube

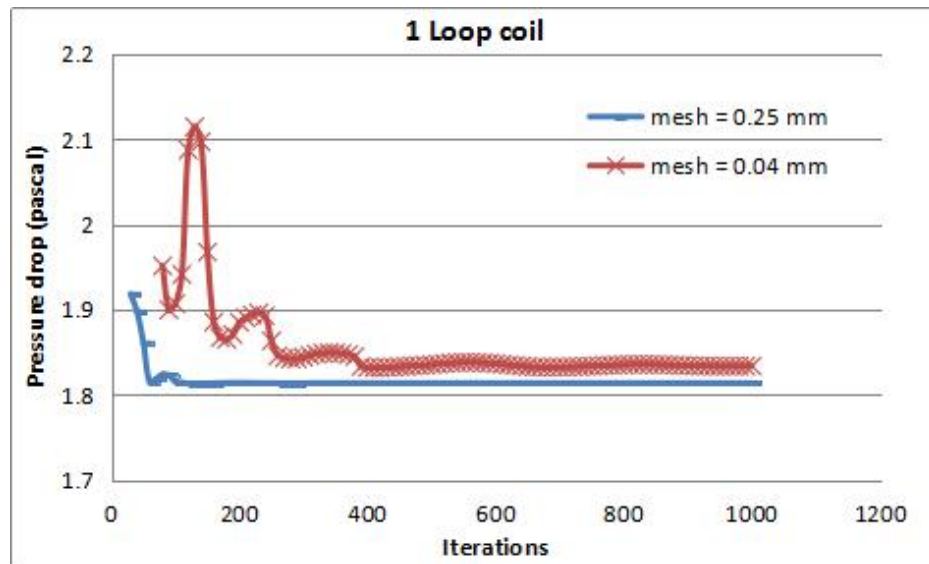


**Figure 3.** Solution convergence/1 loop coil

Figure 4 and Figure 5 represent the computed values of the pressure drop, shown in Table 1 and Table 2, versus the applied grids size.

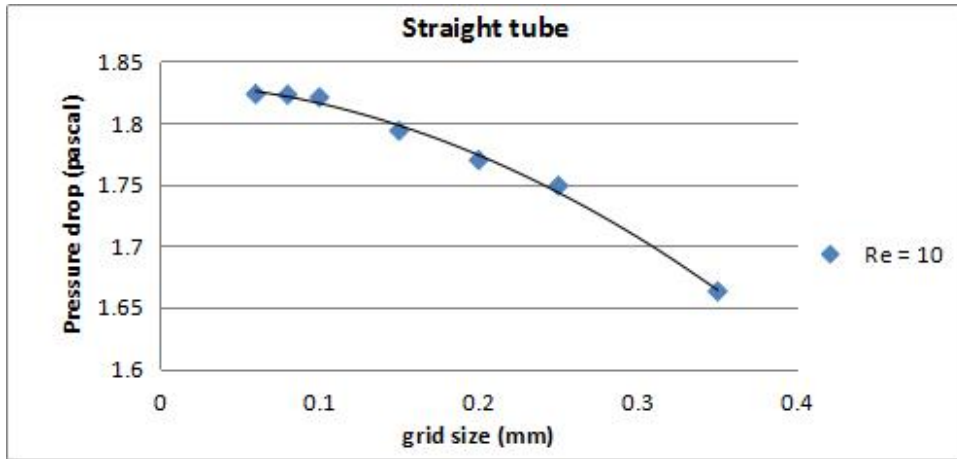


Figure 4. Computed pressure drop for (Reynold No. = 10) versus grid size / Straight tube

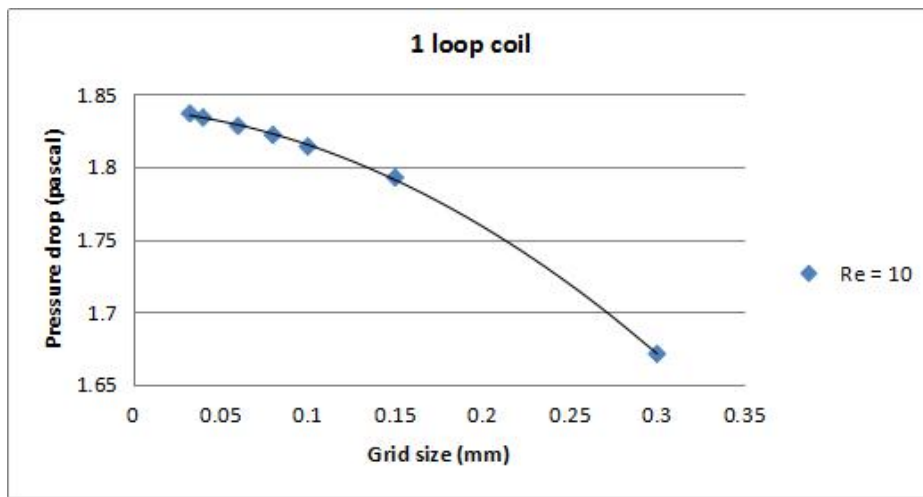


Figure 5. Computed pressure drop for (Reynold No. = 10) versus grid size/1 loop coil

In order to calculate the exact solution, the following approximation was applied for error estimation by assuming the solution is at grid cell falling in the range between 0.08 mm and 0.06 mm for a straight tube and the range between 0.04 mm and 0.0325 mm for a case of 1 loop coil, thus:

$$F1 - Fe = \frac{\Delta X_1^2 (F1 - F2)}{(\Delta X_1^2 + \Delta X_2^2)}$$

where :

F1 & F2 (straight tube) = Computed pressure drop at grid cells (0.08 & 0.06 )

F1 & F2 (1 loop coil) = Computed pressure drop at grid cells (0.04 & 0.0325 )

Fe = exact solution

$\Delta x_1$  &  $\Delta x_2$  = grid cell size

Applying the computed values in the equation above gives:

Fe = 1.823173 Pascal (straight tube)

Fe = 1.835682 Pascal (1 loop coil)

In similar way, (Fe) was calculated for other grid cells and the results are shown in Table 3 and Table 4

Table 3. Relative error of other grids from the exact solution at 0.06 mm grid

Grid size/ Straight tube	Fe	Relative error to 0.06 & 0.08 value
0.06 & 0.08	1.823173	
0.08 & 0.1	1.822045	0.0006187
0.1 & 0.15	1.812399	0.0059094
0.15 & 0.2	1.784974	0.0209515

**Table 4.** Relative error of other grids from the exact solution at 0.0325 mm grid

Grid size/ Single loop coil	Fe	Relative error to 0.0325 & 0.04 value
0.0325 & 0.04	1.835682	
0.04 & 0.06	1.832176	0.00190
0.06 & 0.08	1.822348	0.00726
0.08 & 0.1	1.818844	0.00917

## Results and Discussion

The results of the numerical error study has shown limited changes for the calculated pressure drop upon using 0.1 mm grid size. Hence, all further computations in this study were conducted using 0.1 mm grid cell size, 3d and second order upwind. Enough number of iterations were applied for all the cases studied to get the required accuracy

### Effect of using helical coil on the pressure drop

The pressure drop has been computed for a straight tube, single loop coil and two loops coil in two positions as stated above. Figure 6 illustrates the trend of pressure drop increase downstream the tube with increasing Reynolds number (increasing velocity of the fluid with constant density and viscosity) for all studied cases. Figure 6 illustrates a pressure drop increase due to effect of using curvature section is more obvious when increasing Reynolds number (fluid velocity).

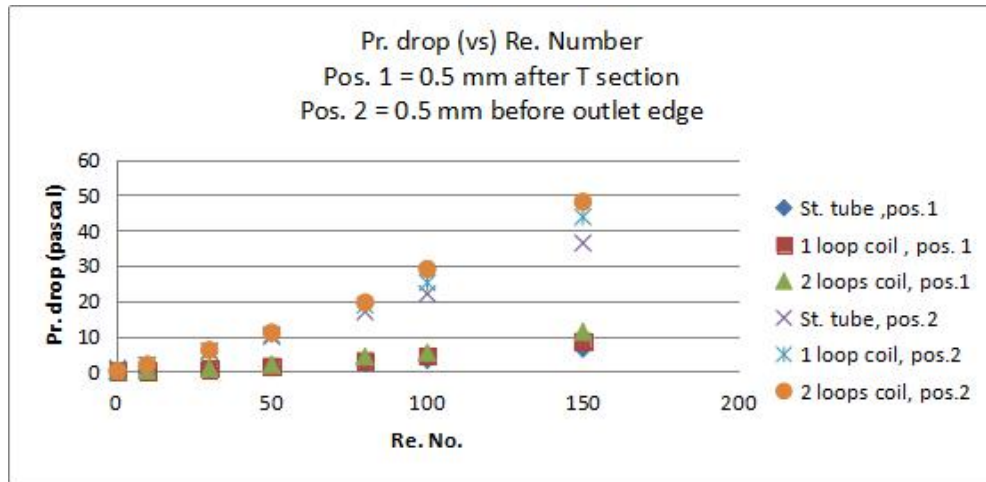


**Figure 6.** Pressure drop versus Reynolds number–Ambient air

**Figure 7** illustrates the effect of using helical coil on the pressure drop at a selected position for two fluids (air and water).

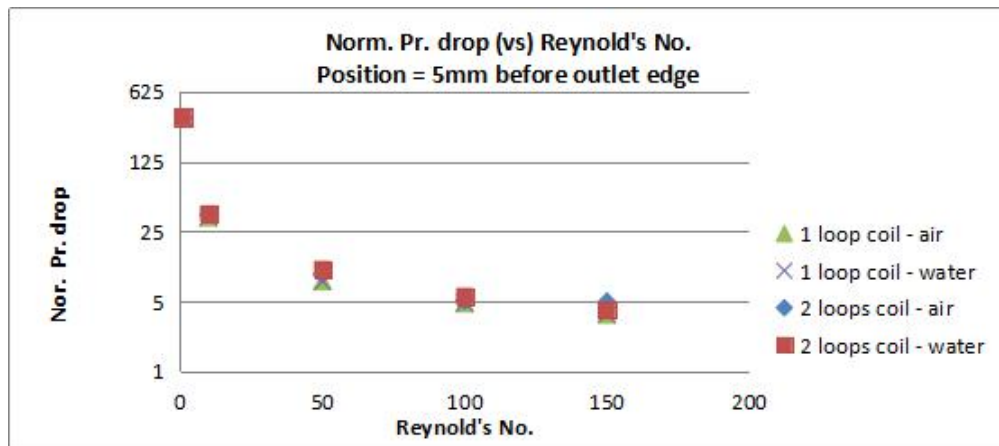


**Figure 7.** Normalized pressure drop (vs.) Reynolds No. For two fluids (air & water)  
where: norm. press. drop =  $\Delta p / (2 \rho u^2)$

The computed normalized values of the pressure drop are shown in Table 5 where slightly higher values were

observed for water. Although the difference is very small, this result indicates that pressure drop, produced from using helical coil, is more effective in the case of liquids.

**Table 5.** Computed normalized values of the pressure drop for single loop coil

Reynolds number	Normalized press. drop/ 1 loop coil		Normalized press. drop/ 2 loops coil	
	Water	Air	Water	Air
1	342.5	340.9	345.4	342.3
10	34.88	34.71	37.6	36.9
50	8	7.97	10.5	9.3
100	4.83	4.81	5.65	5.13
150	3.73	3.723	4.13	4.97

Figure 8 illustrates the total pressure contours, 1 loop coil, at position 5 mm before the outlet edge.

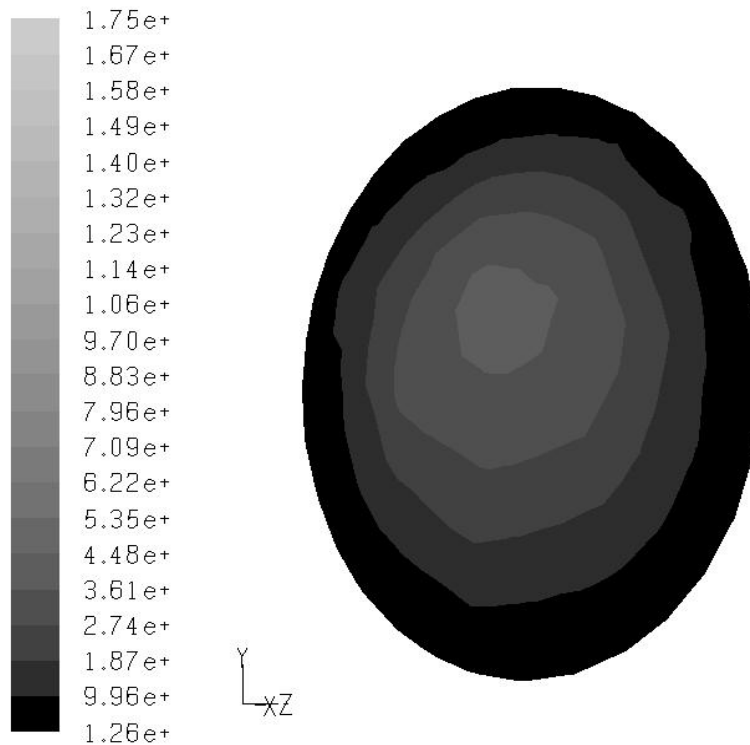


**Figure 8.** Contours of total pressure at position 5 mm before outlet edge

### Pressure drop in the curved tube section

In order to describe the flow in the tube curved section, the terms of cylindrical coordinates were applied for this purpose. When fluid flows through a curved tube, it experiences a positive pressure gradient arising in the radial direction due to the centrifugal force, which can be expressed by the following equation<sup>[3]</sup>.

$$\Delta p_{\text{radial}} = 2 \rho u^2 (d/D)$$

where:  $d$  = tube diameter,  $D$  = coil diameter =  $4d$  (in our case),  $u$  = average velocity

The pressure drop in the axial direction can be expressed by the following equation<sup>[3]</sup>:

$$\Delta p_{\text{axial}} = 4 f_c L \rho u^2 / 2 d$$

where:  $L$  = length of coil

$f_c$  = friction factor of the curved tube, can be expressed by the following empirical equation<sup>[3]</sup>:

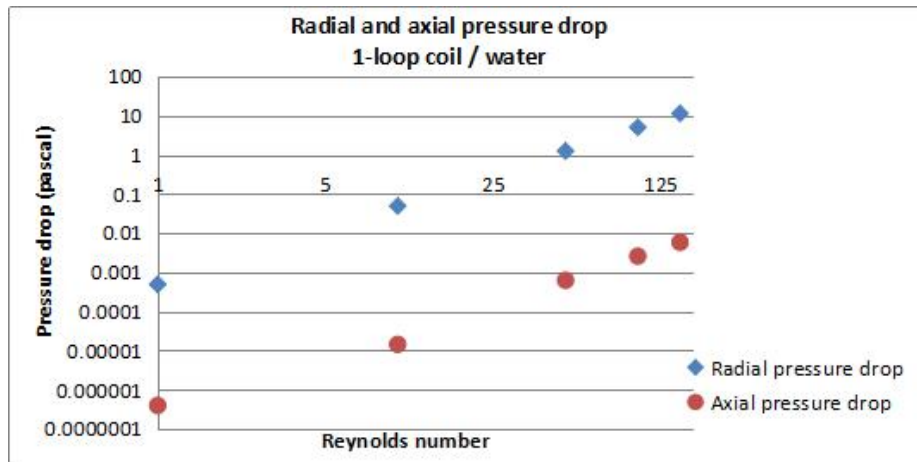
$$f_c = f [ 1 + (0.09 N_D^{1.5}) / (70 + N_D) ]$$

$N_D$  = Modified dean number =  $2 (Re)^2 (aa/LL)$

Where:  $aa$  = Radius of the tube,  $LL$  = Radius of the curvature of the curved tube

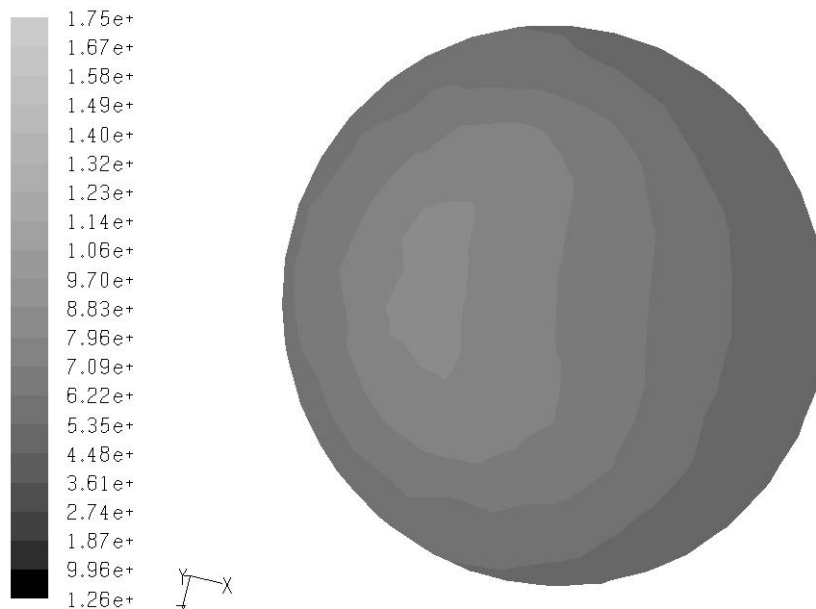
$f = 16/Re$ , in the case of laminar flow

Figure 9 illustrates the computed radial and axial pressure drop, single loop coil, at position (iso surface,  $\theta = 270^\circ$ ) of the coil curve.



**Figure 9.** Radial and axial pressure drop versus Reynolds number at position ( $\theta = 270^\circ$ ) of the curve/water

The values of radial and axial pressure drop were calculated based on the magnitude of velocity which was computed as an average for iso surface taken at the position mentioned above. Figure 9 illustrates that higher values were obtained for the radial pressure drop in comparison to the axial pressure drop. This result can be attributed to the secondary motion that produced from the centrifugal force which acts outward from the centre of curvature on the fluid elements. This motion produces almost uniform pressure gradient at normal lines parallel to the centre axis (axis of symmetry). In contrast, the axial velocity is much faster in the core region, which means limited pressure gradients in other directions. **Figure 10** illustrates the contours of total pressure at position (iso surface,  $\theta = 270^\circ$ ) of the curve.



**Figure 10.** Contours of total pressure at position ( $\theta = 270^\circ$ ) of the curve

### Effect of using the single loop helical coil on the heat transfer

The two inlets into the T-junction have been set at different temperatures in order to extract the effect of using the helical coil on the heat transfer. Water has been introduced with the same velocity 0.025 m/s into both T-junction inlets but with different temperature at the bottom inlet for each case studied (325, 350, 375, 400 and 450 K), while the top inlet kept with the same temperature (300 K). Although uniform heat capacity and thermal conductivity were assumed in the mathematical description, all parameters (density, viscosity, specific heat and thermal conductivity) change with temperature has been taken into consideration in which a linear interpolation (piecewise-linear) has been set in Fluent to calculate the correction needed with temperature change.

**Table 6** illustrates the computed values of the temperature at the specified position as well as the physical parameters at that place and the calculated Prandtl number.

**Table 6.** Computed temperature, physical parameters and Prandtl Number at position ( $x = 5\text{mm}$ ) before outlet edge

Temp. of bott. inlet	Straight tube/ water , 0.025 m/s					1 loop coil/ water , 0.025 m/s				
	Calc. temp. at $x$ , Ko	$\mu$ kg/m. s	Cp J/ kg. Ko	$\lambda$ W/m. Ko	Prandtl No.	Calc. temp. at $x$ , Ko	$\mu$ kg/m. s	Cp J/ kg. Ko	$\lambda$ W/m. Ko	Prandtl No.
325	312.4	6.63E-04	4065.4	0.63178	4.26	312.3	6.64E-04	4065	0.63169	4.27
350	324.7	5.43E-04	4065.9	0.64582	3.42	324.5	5.45E-04	4065.9	0.64536	3.43
375	336.7	4.45E-04	4066	0.65747	2.75	336.6	4.64E-04	4066	0.65684	2.75
400	349.0	3.76E-04	4068.3	0.66727	2.29	348.8	3.77E-04	4068.2	0.66713	2.30
450	373.5	2.82E-04	4082.7	0.6811	1.69	373.2	2.83E-04	4082.4	0.68098	1.69

**Figure 11** illustrates Prandtl number change with the normalized values of inlet temperature at the bottom inlet of the T-junction. The obtained values of Prandtl number are almost identical for a straight tube and the 1 loop coil while an increase in the calculated values was observed when applying 2 loops coil. This effect is expected to be more obvious upon increasing the number of loops of the helical coil into more than 2.

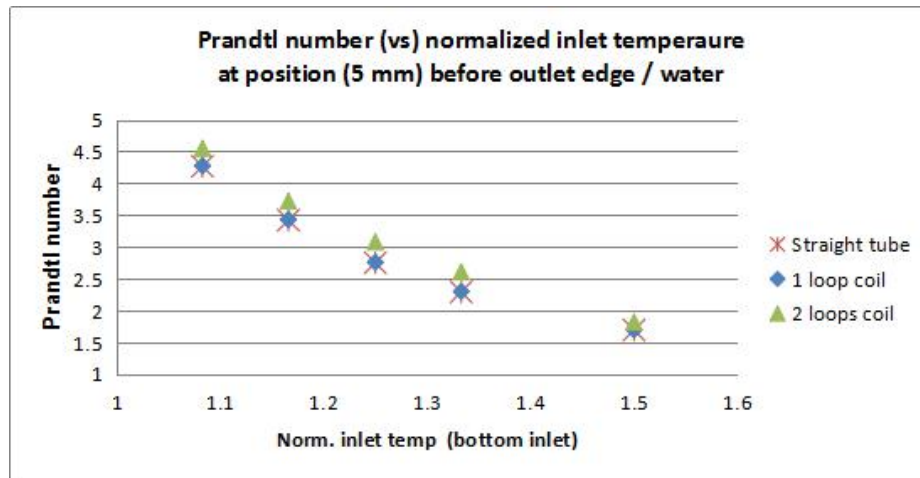


**Figure 11.** Computed Prandtl number versus the normalized temperature ( $T/300$ ) of the bottom inlet at water velocity = 0.025 m/s

### Effect of using single loop helical coil on the mass transfer

The effect of using the coil on mass transfer has been studied by introducing a mixture of (ethanol–water) into the bottom inlet of the T-junction, while pure water was introduced into the top inlet with the same velocity of bottom inlet ( 0.025 m/s). Four combinations of (Ethanol–water) were used to study the case for both the straight tube and the single loop coil, and the Schmidt number was calculated at position ( $x = 5\text{ mm}$ ) before the outlet edge. The study was achieved with assumption of similar temperature for both inlets (300 K). Species model and the energy equation have been switched on in Fluent. All physical parameters have been set in Fluent as (mixing law) in order to consider the effect of mixing on the parameters change, except the value of liquid diffusivity for the (Ethanol–water) mixture which was taken constant ( $128 \times 10^{-11} \text{ m}^2/\text{s}$  at 298 K and 1 atm); however, it was corrected according to the computed temperature in each case<sup>[18]</sup> in order to be used for calculating Schmidt number. The computed temperatures at the specified position were nearly (300 K) for straight tube and the single loop coil, while 302 K was calculated in the case of 2 loops coil.

**Table 7** illustrates the parameters calculated at the specified position for a straight tube and 1 loop coil.

**Table 7.** Computed phys. Prop. & Schmidt number at position ( $x = 5\text{ mm}$ ) before outlet edge

Mass fraction of ethanol in the bottom inlet stream	Straight tube					
	Computed values at position (5 mm) before outlet edge					
	$\mu$ kg/m. s	$\rho$ kg/m <sup>3</sup>	Dk m <sup>2</sup> /s	Schmidt number	Mass fraction of ethanol	Mean molecular weight

0.1	0.00101274	985.3612	1.27146E-09	808.348	0.0495	18.5744
0.25	0.00102696	967.2006	1.27146E-09	835.087	0.12161	19.456
0.5	0.00104969	939.521	1.27062E-09	879.305	0.23698	21.053
0.75	0.00107127	914.6686	1.27002E-09	922.198	0.34652	22.8335
<b>Single loop coil</b>						
<b>Mass fraction of ethanol in the bottom inlet stream</b>	<b>Computed values at position (5 mm) before outlet edge</b>					
	$\mu$ kg/m. s	$\rho$ kg/m <sup>3</sup>	Dk m <sup>2</sup> /s	Schmidt number	Mass fraction of ethanol	Mean molecular weight
0.1	0.001012891	985.1639	1.27143E-09	808.65	0.05	18.583
0.25	0.001026949	967.2111	1.27146E-09	835.071	0.122	19.455
0.5	0.0010496	939.5359	1.27146E-09	878.63	0.237	21.05
0.75	0.001071217	914.7227	1.27146E-09	921.052	0.346	22.829

Figure 12 illustrates an increase in Schmidt number values with increasing the mass fraction of ethanol in the bottom inlet stream for all cases studied. The calculated values of Schmidt number were almost identical for a straight tube and 1 loop coil, while an increase in the calculated values was observed for 2 loops coil. This result is expected to be more obvious upon increasing the number of loops of the helical coil and is attributed to increase in the diffusion coefficient as a result of developed mixing.

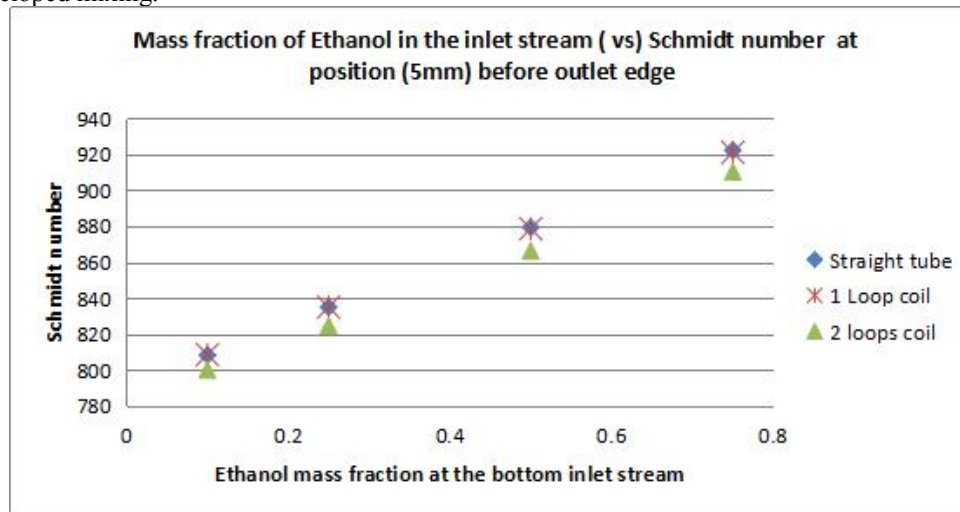


Figure 12. Schmidt number (vs) mass fraction of ethanol in the inlet stream

## Conclusions

This study was devoted to elucidate the effect of using a helical coil on the transport processes. Important findings are highlighted in the following points:

- Larger values of computed pressure drop were obtained upon applying single loop coil compared with a straight tube. The computed pressure drop becomes higher upon applying 2 loops coil. This result became more obvious with increasing the velocity of air in the tube.
- The normalized values of the pressure drop for single loop coil and 2 loops coil were obtained slightly higher for the case of water. This result may indicate the use of helical coil is more effective in the case of liquids. Nevertheless, this conclusion needs to be verified when using multi loops coil.
- Higher values of radial pressure drop were obtained in comparison to the axial pressure drop in the coil section. This result is attributed to the effect of the secondary motion that produced from the centrifugal force which acts outward from the centre of curvature on the fluid elements.
- The computed values of Prandtl number and Schmidt number seemed to be identical for both straight tube and single loop coil. This result indicates a very limited effect produced from applying single loop coil on heat and mass transfer processes. The effects were more obvious upon applying 2 loops coil interpreted by higher values of Prandtl number and lower values of Schmidt number.
- More differences of the computed values could be obtained if the interaction of heat and mass transfer may be taken into consideration. In other word, introducing a hot (ethanol-water) mixture at the bottom inlet and ambient water in

the top inlet could lead to different values of Schmidt number.

- It is expected the effect will be more obvious on the heat and mass transfer when using a helical coil with more than two loops. This is targeted for future work in which the computations should be conducted through a powerful work station.

## References

1. Naphon P, Wongwises S. A review of flow and heat transfer characteristics in curved tubes. *Renewable and Sustainable Energy Reviews* 2006; 10(5): 463–490.
2. Dean WR. Note on the motion of fluid in a curved pipe. *Philosophical Magazine* 1927; 4(20): 208–223.
3. Vashisth S, Kumar V, Nigam KDP. A review on the potential applications of curved geometries in process industry. *Industrial & Engineering Chemistry Research* 2008; 47(10): 3291–3337.
4. Koray Palazoglu T, Sandeep KP. Computational fluid dynamics modelling of fluid flow in helical tubes. *Journal of Food Process Engineering* 2002; 25(2): 141–158.
5. Kumar V, Saini S, Sharma N, et al. Pressure drop and heat transfer study in tube-in-tube helical heat exchanger. *Chemical Engineering Science* 2006; 61(13): 4403–4416.
6. Kumar V, Aggarwal M, Nigam KDP. Mixing in curved tubes. *Chemical Engineering Science* 2006; 61(17): 5742–5753.
7. Kumar PC, Kumar J, Tamilarasan R, et al. Heat transfer enhancement and pressure drop analysis in a helically coiled tube using Al<sub>2</sub>O<sub>3</sub>/water nanofluid. *Journal of Mechanical Science and Technology* 2014; 28(5): 1841–1847.
8. Gomaa A, Aly W, Omara M, et al. Correlations for heat transfer coefficient and pressure drop in the annulus of concentric helical coils. *Heat Mass Transfer* 2014; 50(4): 583–586.
9. Hasabnis NS, Ranade V. Flow and heat transfer in a pinched helical coil. *Indian Chemical Engineer* 2014; 57(1): 1–14.
10. Nada SA, El Shaer WG, Huzayin AS. Heat transfer and pressure drop characteristics of multitubes in tube helically coiled heat exchanger. *JP Journal of Heat and Mass Transfer* 2014; 9: 173–202.
11. Mandal MM, Nigam KDP. Experimental study on pressure drop and heat transfer of turbulent flow in tube in tube helical heat exchanger. *Industrial & Engineering Chemistry Research* 2009; 48(20): 9318–9324.
12. Mhaske GB, Palande DD. Experimental and CFD analysis of tube in tube helical coil heat exchanger. *International Journal of Engineering Research & Technology* 2015; 4(8): 360–365.
13. Heo J, Chung B. Influence of helical tube dimensions on open channel natural convection heat transfer. *International Journal of Heat and Mass Transfer* 2012; 55(11–12): 2829–2834.
14. Ranjbar SF, Seyyedvalilu MH. The effect of geometrical parameters on heat transfer coefficient in helical double tube exchangers. *Journal of Heat and Mass Transfer Research* 2014; 1: 75–82.
15. Jayakumar JS, Mahajani SM, Mandal JC, et al. Experimental and CFD estimation of heat transfer in helically coiled heat exchangers. *Chemical Engineering Research and Design* 2008; 86(3): 221–232.
16. Jassim E. Spiral coil heat exchanger-experimental study. Paper No. 107-Proceedings of the 3rd International Conference on Fluid Flow, Heat and Mass Transfer, Ottawa, Canada, 1–7 (2016)
17. Abdul-Majeed WS, Zimmerman WB. Computational modelling of the hydride generation reaction in a tubular reactor and atomization in a quartz cell atomizer. *Journal of Analytical Sciences, Methods and Instrumentation* 2012; 2: 126–139.
18. Robert H. Perry, Perry's chemical engineers handbook , pp (3-258) , 6th edition, Mc Graw Hill.